Available online at www.sciencedirect.com
ScienceDirect
Trans. Nonferrous Met. Soc. China 32(2022) 3767−3779
Transactions of Nonferrous Metals Society of China
www.tnmsc.cn

Suspension roasting process of vanadium-bearing stone coal: Characterization, kinetics and thermodynamics

Shuai YUAN[1,2], Yong-hong QIN[1,2], Yong-peng JIN[1,2], Yan-jun LI[1,2]

1. School of Resources and Civil Engineering, Northeastern University, Shenyang 110819, China;
2. National−Local Joint Engineering Research Center of High-efficient Exploitation Technology for Refractory Iron Ore Resources, Shenyang 110819, China

Received 22 November 2021; accepted 19 April 2022

Abstract: The thermodynamics, kinetics, phase transformation, and microstructure evolution of vanadium-bearing stone coal during suspension roasting were systematically investigated. Thermodynamic calculations showed that the carbon in the stone coal burned and produced CO_2 in sufficient oxygen during roasting. The mass loss of stone coal mainly occurred within the temperature range from 600 to 840 °C, and the thermal decomposition reaction rate increased to the peak at approximately 700 °C. Verified by the Flynn−Wall−Ozawa (FWO) and Kissinger−Akahira−Sunose (KAS) methods, the thermal decomposition reaction of stone coal was described by the Ginstling−Brounshtein equation. The apparent activation energy and pre-exponential factors were 136.09 kJ/mol and 12.40 s^{-1}, respectively. The illite in stone coal lost hydroxyl groups and produced dehydrated illite at 650 °C, and the structure of sericite was gradually destroyed. The surface of stone coal became rough and irregular as the temperature increased. Severe sintering occurred at the roasting temperature of 850 °C.

Key words: vanadium-bearing stone coal; thermodynamics; thermal decomposition kinetics; phase transformation; microstructure evolution

1 Introduction

As a unique resource in China, stone coal is described as a black sedimentary combustible organic rock generated in the early Proterozoic and early Paleozoic [1,2]. Stone coal is generally gray-black or dark gray, with a dim luster and uniform structure, and is similar in appearance to limestone or carbonaceous shale [3]. The mass fractions of carbon, volatiles, and ash in stone coal are generally 10%−15%, 3%−7%, and 70%−88%, respectively. Stone coal is considered as a fuel with high ash, high sulfur, and low carbon [2], which can be used for thermal power generation. Meanwhile, the residual slag after combustion can be used to produce bricks, tiles, cement and other building materials. Stone coal can be used to extract vanadium, selenium, nickel, molybdenum, and humic acid. The humic acid extracted from stone coal can be used as a fertilizer, soil nutrient, or soil conditioner. As a typical vanadium resource, vanadium content in stone coal generally varies from 0.3% to 1.2% [1,2]. In addition, the grades of other associated elements such as copper, molybdenum, silver, uranium, cadmium, germanium, gallium, zinc, selenium, platinum, and gold in the stone coal are low [1,2].

In China, the vanadium in stone coal mainly exists in the mica lattice in isomorphic form [4−6]. It is difficult to achieve multiple vanadium extraction using a single conventional beneficiation

Corresponding author: Yong-hong QIN, Tel: +86-13898105881, E-mail: qyh_neu@163.com
DOI: 10.1016/S1003-6326(22)66056-4

method, such as gravity concentration and flotation separation [7−12]. Due to the particular occurrence state of vanadium in stone coal, it is necessary to transform the structure of vanadium-bearing minerals and the occurrence state of vanadium in stone coal via pretreatment technology [5,6]. As a well-developed pretreatment technology, roasting is widely used to develop and utilize various refractory mineral resources in mineral processing [13−20]. For a long time, roasting has been one of the key methods in extracting vanadium from stone coal [14,15], which determines the leaching efficiency of vanadium. The traditional process of extracting vanadium from stone coal is sodium roasting−leaching [1,3]. Researchers have gradually proposed various technologies such as calcification roasting, blank roasting, and compound additive roasting [1,3]. Since there are no additives and polluting gas, blank roasting has received great attention [1,3]. The traditional roasting−leaching process shows disadvantages of serious environmental pollution, low stone coal conversion rate, low recovery rate, slow reaction speed, easy sintering, poor product uniformity. Meanwhile it is difficult to apply on a large scale [1,14,15,21−24]. In order to overcome these problems, a suspension roasting technology was proposed [16−20]. This technology involves heating vanadium-bearing stone coal in suspension fluidization to transform V^{3+} to V^{4+} or V^{5+}. Compared with the traditional process, this process has the characteristics of wide adaptability to raw ore, uniform quality of roasted product, high recovery rate, low energy consumption in production, and no pollution. It has been widely used in developing and utilizing a variety of complex and refractory mineral resources.

As a low-grade polymetallic ore with complex composition, many complex chemical reactions occur during the suspension roasting process of stone coal. It is significant for extracting vanadium from stone coal to analyze the thermodynamics of this multivariate complex system, determine the possible reactions in the suspension roasting process, and control the reaction conditions. Several researches on kinetics of static roasting for stone coal have been carried out [25,26], but it is difficult to guide the suspension roasting industrial application and production of stone coal. In this study, the Gibbs free energies of the possible chemical reactions during stone coal suspension roasting were calculated by HSC Chemistry software to determine whether the reaction could proceed spontaneously. According to the thermal decomposition rate of stone coal obtained by the TG−DTG−DSC characterization, the best kinetic model was calculated and fitted by the least square method. Thus, the reaction mechanism in the process of stone coal decomposition was obtained. Besides, the phase transformation and micro-structure evolution during the suspension roasting of stone coal were analyzed by using the X-ray diffraction (XRD), Fourier transforms infrared spectroscopy (FTIR spectroscopy), and scanning electron microscopy (SEM).

2 Experimental

2.1 Materials and experiment

The stone coal raw ore used in this study was collected from Dunhuang, Gansu Province, China. The chemical composition of stone coal is listed in Table 1. The mass fractions of vanadium, carbon, SiO_2, and Al_2O_3 were 0.98%, 14.15%, 63.7%, and 10.46%, respectively. In addition, the CaO, K_2O, and MgO contents were 3.45%, 2.19%, and 1.19%, respectively. Figure 1 shows the X-ray diffraction (XRD) pattern of stone coal. The characteristic diffraction peaks of quartz, calcite, and goethite were observed, and the diffraction peaks of mica were basically covered by quartz. Then, 20 g of vanadium-bearing stone coal with a particle size of <0.5 mm was placed into the suspension roasting furnace, and the heating rate of the furnace was 10 °C/min. The roasting experiments of ore samples were carried out in a suspension roasting system that was mainly composed of a gas supply system, heating reaction system, temperature control system, and tail gas treatment system. Compared with other static roasting devices, such as muffle furnaces, this device can have various combinations or a single roasting gas atmosphere. The materials can

Table 1 Chemical composition of vanadium-bearing stone coal (wt.%)

SiO_2	Na_2O	V_2O_5	P_2O_5	S	Al_2O_3
63.70	0.87	0.98	0.57	0.44	10.46
CaO	TFe	K_2O	MgO	C	Ignition loss
3.45	3.00	2.19	1.19	14.15	18.40

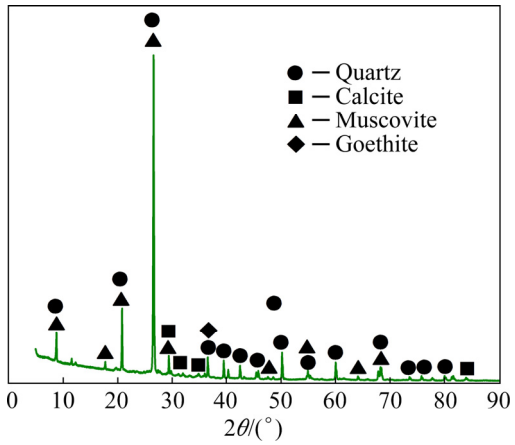

Fig. 1 XRD pattern of vanadium-bearing stone coal

be roasted more completely in the flowing gas atmosphere, and the roasting effect is better.

2.2 Sample characterization

In this work, thermal analysis of stone coal during thermal decomposition was performed by using an SDTQ 600 thermal analyzer (TA Instrument Company, United States of America). Samples placed in corundum crucibles were roasted at heating rates of 5, 10, 15, and 20 °C/min from 20 to 1200 °C. The phase transformation during roasting process was identified using X-ray diffraction analysis (Smartlab, Rigaku, Japan) at a pipe voltage of 45 kV and a pipe current of 200 mA. The equipment parameters were as follows: 2θ diffraction angle range from 5° to 90°, scanning rate of 12 (°)/min, Cu target radiation, nickel filter, and solid-state detector. A 380 Fourier transform infrared (FT-IR) spectrometer (Thermo, USA) was used to reveal the structural variation of stone coal during suspension roasting. The KBr powder and roasted products (with mass ratio of 100:1) were ground in an agate mortar and pressed into flakes. The analyses of infrared spectra were conducted at a scan resolution of 4 cm^{-1} and scan times of 128. The microstructure of vanadium-bearing stone coal during suspension roasting was evaluated under a scanning electron microscope (SEM) (ULTRA PLUS, Zeiss, Germany). Since the roasted product was not conductive, an Au film with thickness about 10 nm was coated on the surface of the roasted products. The micromorphology of vanadium-bearing stone coal during suspension roasting was obtained at an acceleration voltage of 15 kV.

2.3 Analysis of solid thermal decomposition kinetics

In general, the thermal decomposition process of a solid can be summarized as A(s)→B(s)+C(g). The conversion ratio at any time t or temperature T of the decomposition process [27] is defined as α:

$$\alpha = \frac{m_0 - m_t}{m_0 - m_f} \tag{1}$$

where m_0, m_t, and m_f are the initial sample mass (g), sample mass (g) at time t or temperature T, and sample mass (g) at the end of the reaction, respectively.

The relationships among conversion ratio α, reaction rate $d\alpha/dT$, time, and temperature were described by using the kinetic mechanism function or kinetic model. In this work, 15 common kinetic mechanism functions of thermal decomposition are listed in Table 2 [27]. $f(\alpha)$ is the differential form of the mechanism function, and $G(\alpha)$ is the corresponding integral form.

The kinetic equation of pyrolysis process [27] is expressed as

$$\frac{d\alpha}{dt} = k(T)f(\alpha) \tag{2}$$

where $k(T)$, t, and $f(\alpha)$ are the rate constant (s^{-1}), pyrolysis time (s), and reaction mechanism function, respectively.

According to the Arrhenius equation, the rate constant can be described by

$$k(T) = A\exp\left(-\frac{E_a}{RT}\right) \tag{3}$$

where T and R are the thermodynamic temperature (K), and molar gas constant (8.314 J/(mol·K)), respectively; E_a is the activation energy (J/mol); A is the frequency factor or preexponential factor (min^{-1}).

The most likely mechanism and kinetic parameters of stone coal roasting were identified by using the logarithmic form of the modified Coats−Redfern method [27]:

$$\ln\frac{G(\alpha)}{T^2} = \ln\left(\frac{AR}{\beta E_a}\right) - \frac{E_a}{RT} \tag{4}$$

where $G(\alpha)$ is the rate constant (s^{-1}); β is the heating rate (K/min).

Based on the equal conversion method, the isoconversional methods of Flynn−Wall−Ozawa (FWO) and Kissinger−Akahira−Sunose (KAS) [27]

Table 2 Common differential and integral forms of thermal decomposition kinetic mechanism

Code	Name	$f(\alpha)$	$G(\alpha)$
$R_{1/3}$	Reaction order equation, n=1/3	$(1-\alpha)^{1/3}$	$(3/2)[1-(1-\alpha)^{2/3}]$
$R_{3/4}$	Reaction order equation, n=3/4	$(1-\alpha)^{3/4}$	$4[1-(1-\alpha)^{1/4}]$
$R_{3/2}$	Reaction order equation, n=3/2	$(1-\alpha)^{3/2}$	$2[(1-\alpha)^{-1/2}-1]$
R_2	Reaction order equation, n=2	$(1-\alpha)^2$	$\alpha/(1-\alpha)$
R_3	Reaction order equation, n=3	$(1-\alpha)^3$	$(1/2)[(1-\alpha)^{-2}-1]$
A_1	Avrami–Erofeev equation, n=1	$1-\alpha$	$-\ln(1-\alpha)$
$A_{3/2}$	Avrami–Erofeev equation, n=3/2	$(1-\alpha)[-\ln(1-\alpha)]^{1/3}$	$(3/2)\ [-\ln(1-\alpha)]^{2/3}$
A_2	Avrami–Erofeev equation, n=2	$(1-\alpha)[-\ln(1-\alpha)]^{1/2}$	$2\ [-\ln(1-\alpha)]^{1/2}$
A_3	Avrami–Erofeev equation, n=3	$(1-\alpha)[-\ln(1-\alpha)]^{2/3}$	$3\ [-\ln(1-\alpha)]^{1/3}$
A_4	Avrami–Erofeev equation, n=4	$(1-\alpha)[-\ln(1-\alpha)]^{3/4}$	$4\ [-\ln(1-\alpha)]^{1/4}$
D_1	Parabola law	$1/\alpha$	$\alpha^2/2$
D_2	Valensi equation	$[-\ln(1-\alpha)]^{-1}$	$\alpha+(1-\alpha)\ln(1-\alpha)$
D_5	Z−L−T equation	$(1-\alpha)^{4/3}[(1-\alpha)^{-1/3}-1]^{-1}$	$(3/2)[(1-\alpha)^{-1/3}-1]^2$
D_6	Jander equation	$(1-\alpha)^{2/3}[1-(1-\alpha)^{1/3}]^{-1}$	$(3/2)\ [1-(1-\alpha)^{1/3}]^2$
D_8	G−B equation	$3/2[(1-\alpha)^{-1/3}-1]^{-1}$	$1-2/3\alpha-(1-\alpha)^{2/3}$

were used to verify the apparent activation energy calculated by the Coats−Redfern method:

$$\ln\beta=\ln\left(\frac{AE_a}{RG(\alpha)}\right)-2.315-0.4567\frac{E_a}{RT} \quad (5)$$

$$\ln\frac{\beta}{T^2}=\ln\left(\frac{AR}{E_a}\right)-\frac{E_a}{RT} \quad (6)$$

3 Results and discussion

3.1 Thermodynamic analysis

3.1.1 Reactions of calcium-containing substances in stone coal

The calcium minerals in the vanadium-bearing stone coal used in the test are mainly anhydrite (mainly composed of $CaSO_4$) and calcite (mainly composed of $CaCO_3$). Therefore, the possible chemical reactions during oxidative roasting are shown in Reactions (7)−(14). The standard Gibbs free energies of the above reactions were calculated using the Reaction Equation module in the thermodynamic software HSC chemistry 6.0, as shown in Fig. 2.

$$CaSO_4+2C+H_2O=CaO+2CO_2(g)+H_2S(g) \quad (7)$$

$$CaCO_3=CaO+CO_2(g) \quad (8)$$

$$CaO+V_2O_5=CaV_2O_6 \quad (9)$$

$$2CaO+V_2O_5=Ca_2V_2O_7 \quad (10)$$

$$3CaO+V_2O_5=Ca_3(VO_4)_2 \quad (11)$$

$$CaO+SiO_2=CaSiO_3 \quad (12)$$

$$CaO+Al_2O_3=CaAl_2O_4 \quad (13)$$

$$CaO+SiO_2+Al_2O_3=CaAl_2SiO_6 \quad (14)$$

From Fig. 2, the Gibbs free energy of the reaction in Reaction (7) began to be less than 0 when the temperature was higher than 595 K, which decreased with increasing temperature. When the temperature was higher than 1155 K, the chemical reaction in Reaction (8) could proceed spontaneously. These two chemical reactions were the primary sources of CaO in roasted stone coal. It could be concluded from Fig. 2 that the ΔG^{Θ} of the reaction between CaO and V_2O_5 was lower than that between SiO_2 and Al_2O_3, which suggested that the chemical reactions of Reactions (9)−(11) are easier to occur.

3.1.2 Carbon oxidation

Since the carbon content in stone coal was high, the heat distribution during roasting was affected, resulting in increased acid consumption, which in turn limited the extraction of vanadium from the stone coal. Therefore, it was necessary to decarbonize the stone coal, and the possible reactions of carbon during roasting are shown in Reactions (15)−(18). Figure 2 suggests that the Reactions (15)−(17) can proceed spontaneously at

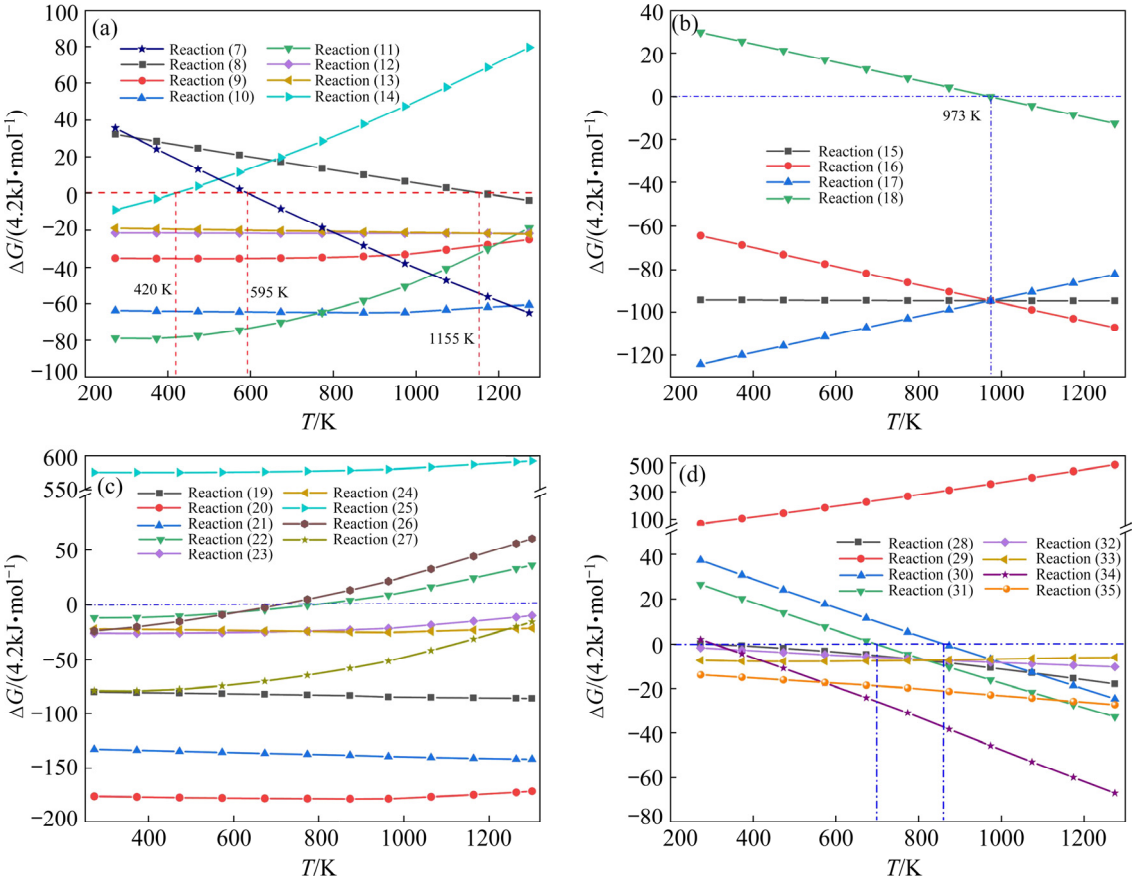

Fig. 2 Gibbs free energy change of chemical reaction in roasting process of stone coal

the temperature from 200 to 1400 K. Furthermore, Reaction (18) might proceed spontaneously only after the temperature exceeded 973 K. CO was generated in insufficient oxygen through Reaction (16), while CO_2 was generated in sufficient oxygen through Reaction (17). Therefore, adequate oxygen is necessary for removing carbon.

$$C+O_2(g)=CO_2(g) \quad (15)$$

$$2C+O_2(g)=2CO(g) \quad (16)$$

$$CO(g)+O_2(g)=CO_2(g) \quad (17)$$

$$C+CO_2(g)=CO(g) \quad (18)$$

3.1.3 Formation of vanadate

The vanadium in the mica lattice is released and oxidized to generate soluble vanadate with the metal oxides in the ore, which is the primary approach for vanadium extraction by roasting–leaching. Therefore, the formation of vanadate and the sequence of vanadate formation are essential for efficient vanadium extraction. Since there were many metals in stone coal, the vanadate that might be generated during roasting is shown in Reactions (19)−(27). Figure 2 shows that the Gibbs free energy change of the reaction between Na_2O and V_2O_5 was the lowest, followed by that between CaO and V_2O_5 then that between MgO and V_2O_5. From Reaction (25), the reaction between Fe_2O_3 and V_2O_5 cannot proceed from 200 to 1400 K. Therefore, in the process of stone coal roasting, the order of difficulty for different metal oxides to generate the same type of vanadate with V_2O_5 is Na_2O>CaO>MgO>Fe_2O_3. The difficulty of forming different vanadates with the same metal oxide and V_2O_5 is orthovanadate > pyrovanadate > metavanadate.

$$V_2O_5+Na_2O=2NaVO_3 \quad (19)$$

$$V_2O_5+3Na_2O=2Na_3VO_4 \quad (20)$$

$$V_2O_5+2Na_2O=Na_4V_2O_7 \quad (21)$$

$$V_2O_5+MgO=Mg(VO_3)_2 \quad (22)$$

$$V_2O_5+MgO=Mg_3(VO_4)_2 \quad (23)$$

$$V_2O_5+2MgO=Mg_2V_2O_7 \quad (24)$$

$$V_2O_5+Fe_2O_3=2FeVO_4 \quad (25)$$

$$V_2O_5+CaO=Ca(VO_3)_2 \quad (26)$$

$$V_2O_5+3CaO=Ca_3(VO_4)_2 \quad (27)$$

3.1.4 Reactions of iron-containing substances in stone coal

According to the multi-element analysis and XRD patterns of raw ore, there was few goethite in the stone coal. The possible reactions of goethite and its reaction products during roasting are shown in Reactions (28)−(35). From Fig. 2, the decomposition reaction of goethite could proceed spontaneously. CO would be generated in insufficient oxygen through the incomplete combustion of carbon in the system. CO might reduce Fe_2O_3 to Fe_3O_4, Fe, or FeO. Meanwhile, Fe_2O_3 was first reduced to Fe_3O_4 (Reaction (34)) when the carbon was excessive. Fe_2O_3 would be reduced to FeO by the carbon in the system when the temperature exceeded 700 K. Fe_2O_3 would be reduced to Fe by the carbon in the system when the temperature rose to 860 K. Besides, the Gibbs free energy change of Reaction (29) was always greater than 0 when oxygen was sufficient, and thus the reaction could not proceed spontaneously.

$$2FeOOH=Fe_2O_3+H_2O \quad (28)$$

$$Fe_2O_3+3CO_2(g)=Fe_2(CO_3)_3 \quad (29)$$

$$Fe_2O_3+1.5C=2Fe+1.5CO_2(g) \quad (30)$$

$$2Fe_2O_3+C=4FeO+CO_2(g) \quad (31)$$

$$Fe_2O_3+3CO(g)=2Fe+3CO_2(g) \quad (32)$$

$$Fe_2O_3+CO(g)=2FeO+CO_2(g) \quad (33)$$

$$6Fe_2O_3+C=4Fe_3O_4+CO_2(g) \quad (34)$$

$$3Fe_2O_3+CO(g)=2Fe_3O_4+CO_2(g) \quad (35)$$

3.2 Thermogravimetric analysis of stone coal

The synchronous thermal analysis of vanadium-bearing stone coal was performed at different heating rates and the results are displayed in Figs. 3−5. According to the results of the TG curves, the roasting process of vanadium-bearing stone coal in the air was divided into three stages. In Stage I, the mass loss in the temperature range of 0−600 °C was small, mainly due to removing adsorbed water from vanadium-bearing stone coal and the decomposition of goethite. In Stage II, a prominent endothermic peak appeared on the DSC curve in the temperature range of 600−840 °C. The minimum value appearing on the DTG curve indicated that the mass change rate of stone coal reached an extreme value. A violent endothermic reaction occurred in the vanadium-bearing stone coal, resulting in rapid mass loss. In this stage, the combustion reaction of carbon, the decomposition of calcite, and the structure destruction of illite and mica mainly occurred. In Stage III, from the DTG

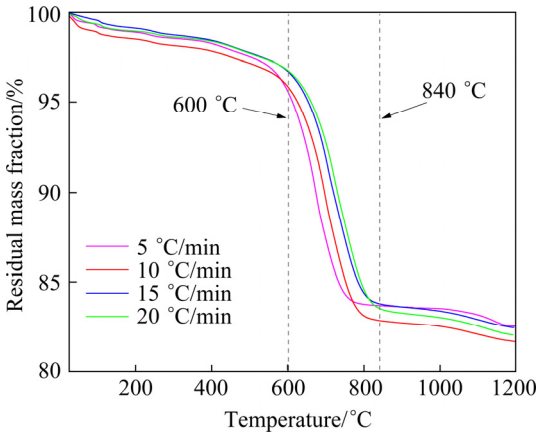

Fig. 3 TG curves of vanadium-bearing stone coal at different heating rates

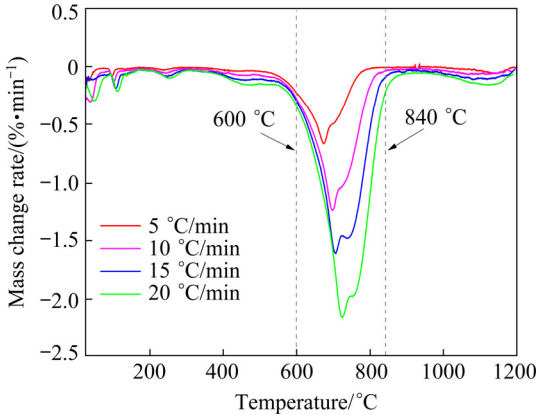

Fig. 4 DTG curves of vanadium-bearing stone coal at different heating rates

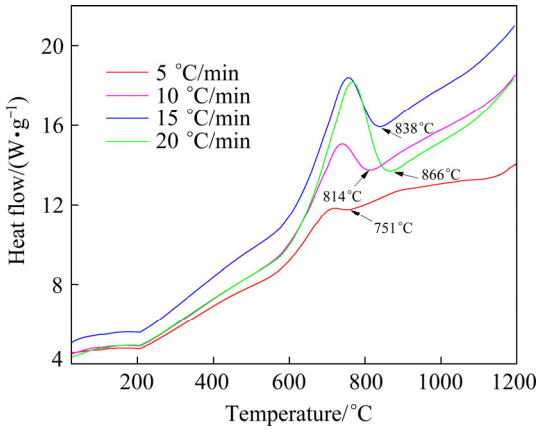

Fig. 5 DSC curves of vanadium-bearing stone coal at different heating rates

and DSC curves, the reaction in the roasting process was finished at temperature >840 °C, and the mass of the sample did not change.

From the TG curves (Fig. 3), it was observed that the major mass loss occurred within the temperature range of 600−840 °C. Different heating rates affected the thermal decomposition noticeably. Since the thermal hysteresis was generated by the uneven heating inside and outside the sample [28] with the increase in heating rate, the mass loss gradually moved towards the high temperature stage. Besides, the DTG curve indicated that the mass loss rate of the stone coal gradually increased with the increase of heating rate, and the temperature of the maximum mass loss rate moved to the high temperature zone. Figure 5 showed that vanadium-bearing stone coal had different degrees of heat absorption and release under different heating rates. The degree of heat absorption of stone coal increased with the increase of heating rate. The stone coal roasting reaction was basically completed at a certain temperature under different heating rates, and the sample mass and heat tended to be stable. When the heat absorption rates were 10 and 20 °C/min, the temperatures were 814 and 866 °C, respectively.

3.3 Conversion ratio and reaction rate of decomposition reaction

The roasting process of the stone coal is considered to be a decomposition reaction. The conversion ratio (α) of the reaction process and the reaction rate were calculated, as shown in Figs. 6 and 7. Figure 6 suggests that the conversion ratio showed a slow upward trend at temperatures lower than 600 °C. The conversion ratio increased rapidly when the temperature rose to 600−800 °C. The conversion ratio tended to remain stable as the temperature exceeded 800 °C. A similar phenomenon could be observed in the relationship curve between the reaction rate and temperature (Fig. 7). The reaction rate was almost zero when the temperature was lower than 600 °C. As the temperature rose above 600 °C, the reaction rate increased rapidly to the peak at approximately 680 °C and then quickly decreased with increasing temperature. The peak value of the reaction rate was improved with the increase of heating rate, and the temperature of the peak value increased gradually.

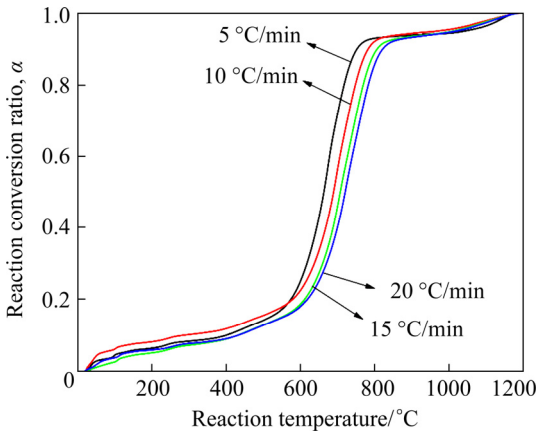

Fig. 6 Conversion ratio of thermal decomposition of stone coal at different heating rates

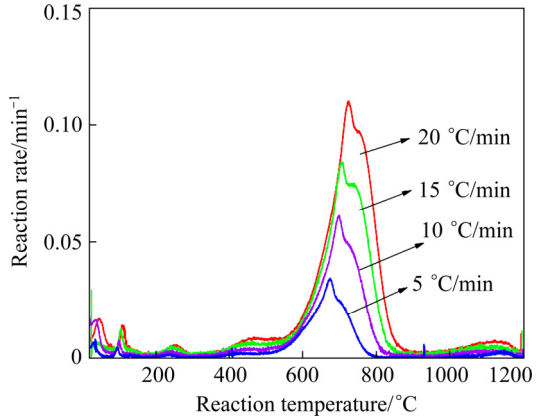

Fig. 7 Reaction rate of thermal decomposition of stone coal at different heating rates

3.4 Parameter calculation of nonisothermal kinetics model

The chemical reaction in the thermal decomposition process was discussed. The kinetic decomposition model of stone coal in the heating process was ascertained through the thermogravimetric analysis of stone coal under different heating rates. The rate constant $f(\alpha)$, apparent activation energy E_a, and preexponential factor A were obtained to clarify the variation of stone coal during roasting and effectively control the decomposition reaction.

According to the C−R temperature integral equation, the correlation coefficients R^2 of different standard thermal decomposition kinetic mechanism functions were calculated by using the equal conversion method, as given in Table 3. From Table 3, Models D_2, D_6, and D_8 have better correlations than the other models, with correlation coefficients over 0.98. The linear fitting results of

Models D_2, D_6, and D_8 are shown in Fig. 8, which indicates that the reaction of stone coal during thermal decomposition can be characterized by the functional model of the diffusion control mechanism.

According to the slope and intercept of the fitting curve, the apparent activation energies of mechanism functions D_2, D_6, and D_8 were obtained, as given in Table 4. The apparent activation energies of mechanism functions D_2, D_6, and D_8 were 128.57, 129.75, and 136.09 kJ/mol, respectively.

The Flynn−Wall−Ozawa (FWO) equation and Kissinger−Akahira−Sunose (KAS) equation verified the apparent activation energy of the reaction to ascertain the most likely reaction mechanism function. According to Eq. (5), the slope of the linear curves between $\ln \beta$ and $1/T$ was $-0.4567E_a/R$ at any conversion ratio α, which was independent of the mechanism function. Therefore, the relationship between $\ln \beta$ and $1/T$ at conversion ratios of 0.3−0.8 is shown in Fig. 9. Based on Eq. (6), the slope of the linear curves between $\ln(\beta/T^2)$ and $1/T$ was $-E_a/R$ at any conversion ratio α. The relationship between $\ln(\beta/T^2)$ and $1/T$ at conversion ratios of 0.3−0.8 is shown in Fig. 10.

Table 5 indicated that the determination coefficient (R^2) values of all samples calculated by the FWO and KAS equations were above 0.98. This implies that the best results are obtained with the FWO and KAS equations. The activation energy calculated using the slope of the fitting line according to the FWO equation varied from 167.82 to 177.13 kJ/mol, while the activation energy calculated using the KAS equation ranged from 161.37 to 170.38 kJ/mol.

Table 3 Calculated results (R^2) of C−R integral equation using equal conversion rate method

Mechanism function	Name	Code	Heating rate/(°C·min^{-1})				Average value
			5	10	15	20	
Chemical reaction	Reaction order equation, n=1/3	$R_{1/3}$	0.98014	0.97283	0.98086	0.98049	0.97858
	Reaction order equation, n=3/4	$R_{3/4}$	0.98506	0.96498	0.98499	0.98282	0.97946
	Reaction order equation, n=3/2	$R_{3/2}$	0.96618	0.92862	0.96441	0.95972	0.95473
	Reaction order equation, n=2	R_2	0.30186	0.27427	0.30936	0.30771	0.29830
	Reaction order equation, n=3	R_3	0.90082	0.84724	0.89716	0.89010	0.88383
Nucleation growth model	Avrami–Erofeev equation, n=1	A_1	0.98195	0.95521	0.98131	0.97818	0.97416
	Avrami–Erofeev equation, n=3/2	$A_{3/2}$	0.97879	0.94615	0.97790	0.97407	0.96923
	Avrami–Erofeev equation, n=2	A_2	0.97457	0.93361	0.97326	0.96843	0.96247
	Avrami–Erofeev equation, n=3	A_3	0.96037	0.88816	0.95709	0.94837	0.93850
	Avrami–Erofeev equation, n=4	A_4	0.92714	0.76634	0.91616	0.89554	0.87630
Diffusion model	Parabola law	D_1	0.97476	0.97787	0.97594	0.97696	0.97639
	Valensi equation	D_2	0.98370	0.97871	0.98450	0.98436	0.98282
	Z−L−T equation	D_5	0.97095	0.94631	0.97454	0.97095	0.96569
	Jander equation	D_6	0.98466	0.97877	0.98539	0.98513	0.98349
	G−B equation	D_8	0.98613	0.97772	0.98671	0.98609	0.98416

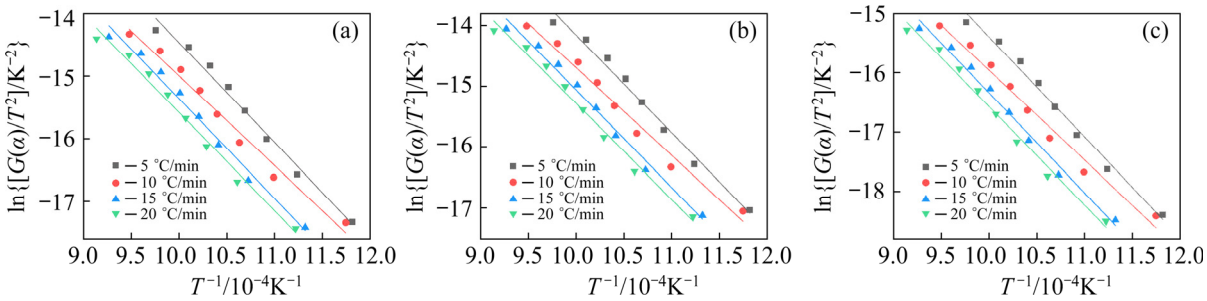

Fig. 8 Fitting curves of different mechanism functions at different heating rates: (a) D_2; (b) D_6; (c) D_8

Table 4 Apparent activation energies and correlation coefficients of D_2, D_6, and D_8

Heating rate/ (°C·min^{-1})	Valensi equation		Jander equation		G−B equation	
	E/(kJ·mol^{-1})	R^2	E/(kJ·mol^{-1})	R^2	E/(kJ·mol^{-1})	R^2
5	132.76	0.9837	133.98	0.9847	140.52	0.9861
10	119.24	0.9787	120.31	0.9788	126.13	0.9777
15	132.2	0.9845	133.43	0.9854	139.96	0.9867
20	130.2	0.9844	131.3	0.9851	137.73	0.9861
Average value	128.57	0.9828	129.75	0.9835	136.09	0.9842

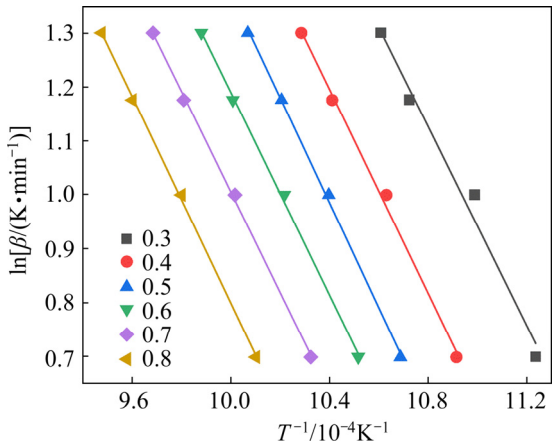

Fig. 9 Fitting curves of FWO equation at different conversion ratios

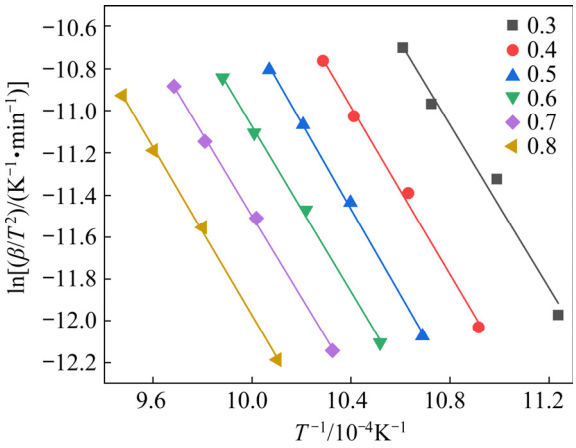

Fig. 10 Fitting curves of KAS equation at different conversion ratios

The average values of activation energies by the FWO and KAS equations were 171.99 and 164.85 kJ/mol, respectively. Both are similar to the activation energy of mechanism D_8 obtained by using the C−R equation. Therefore, the Ginstling−Brounshtein equation was determined to be the most likely function of the thermal decomposition reaction of vanadium-bearing stone coal during roasting, whose integral form and differential form

Table 5 Apparent activation energies and correlation coefficients of FWO and KAS methods at different conversion ratios

Conversion ratio	FWO equation		KAS equation	
	E_a/(kJ·mol^{-1})	R^2	E_a/(kJ·mol^{-1})	R^2
0.3	167.82	0.9837	161.37	0.9805
0.4	172.14	0.9966	165.46	0.9959
0.5	177.13	0.9989	170.38	0.9986
0.6	170.91	0.9987	163.54	0.9984
0.7	169.74	0.9992	162	0.999
0.8	174.23	0.9994	166.36	0.9993
Average value	171.99	0.9961	164.85	0.9953

were $G(\alpha)=1-2/3\alpha-(1-\alpha)^{2/3}$ and $f(\alpha)=3/2[(1-\alpha)^{-1/3}-1]^{-1}$, respectively. The apparent activation energy and preexponential factors were 136.09 kJ/mol and 12.40 s^{-1}, respectively. The results of the kinetic calculation show that the kinetic process of the roasting reaction belongs to the diffusion model. In this study, vanadium-bearing stone coal contains carbonaceous, calcite and other substances, which release large amounts of CO, CO_2 and other gases in the roasting reaction. Gas diffusion outward leads to the formation of a typical porous structure on the surface of vanadium-bearing stone coal, which is consistent with the SEM images of stone coal roasting products.

3.5 Phase transformation and molecular structure variation

X-ray diffraction was carried out to further study the roasted products at different temperatures to better understand the phase transformation of stone coal. As shown in Fig. 11, the goethite in raw ore slowly decomposed into hematite with increasing temperature [29,30]. Previous studies

implied that interlayer and adsorbed water would be removed as a first step during the roasting of illite [28]. The intensity of the characteristic diffraction peak of illite decreased obviously when the temperature was higher than 700 °C, which reflected that the hydroxyl groups of illite were removed during this process, producing a dehydrated illite phase. From Fig. 11, the diffraction peaks of sericite were gradually weakened at 700 °C, meaning that the structure of sericite started to be destroyed [29,30]. In addition, with the increase in roasting temperature, the characteristic diffraction peak of calcite gradually faded and finally disappeared at approximately 800 °C, which suggested that the calcite in the raw ore was completely decomposed. The structures of quartz and muscovite were destroyed with increasing temperature. The intensity of diffraction peak of feldspar first increased and then decreased with increasing temperature, implying that quartz would react with mica to produce the feldspar phase at a low temperature. Feldspar minerals would continue to react with mica at a high temperature.

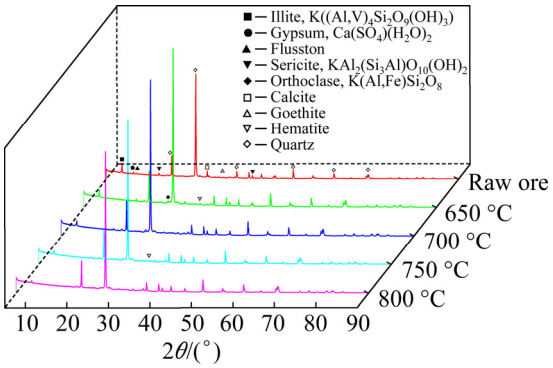

Fig. 11 XRD patterns of raw ore and roasted samples at different temperatures

Figure 12 presents the infrared spectra at different temperatures corresponding to the roasted products. Information on the molecular structure could be obtained from the FTIR spectra to deduce the phase transformation during the roasting process. The absorption peaks at 3693.08 and 3619.15 cm^{-1} in the high-frequency region of the spectra belonged to the telescopic vibration absorption peaks of the outer hydroxyl group and the inner hydroxyl group of vanadium-bearing mica, respectively. When the temperature reached 650 °C, the two absorption peaks disappeared, which indicated that the internal and external hydroxyl groups of mica were entirely removed. The absorption band at 1424.63 cm^{-1} was the distinctive absorption peak of calcite. As the roasting temperature reached 800 °C, the absorption peak of calcite disappeared, indicating that the calcite structure in the raw ore was destroyed [31,32]. The high-strength absorption bands at 1081.21 and 1032.56 cm^{-1} were the stretching vibration peaks of Si—O. The absorption peak at 1032.56 cm^{-1} disappeared at the roasting temperature of 650 °C, indicating that the Si—O bond fractured, and the structure of vanadium-bearing mica began to be destroyed. The shoulder peak at 512.01 cm^{-1} was attributed to the bending vibration of the SO_4^{2-} group. The disappearance of the peak at 512.01 cm^{-1} implied that the anhydrite in stone coal raw ore was reduced.

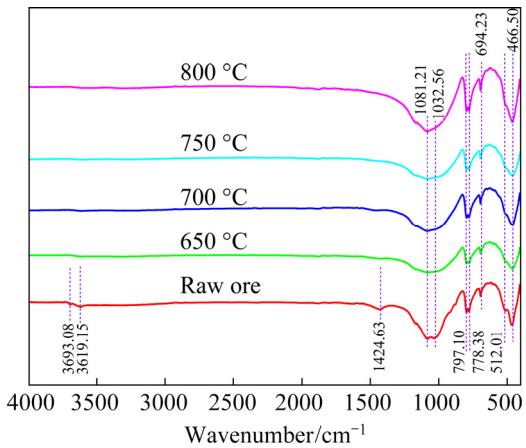

Fig. 12 FT-IR spectra of raw ore and roasted samples at different temperatures

3.6 Microstructure evolution

A scanning electron microscope was employed to analyze the raw ore and roasted products at different temperatures. Figures 13(a_1, a_2) show the morphologies of stone coal raw ore. Many flakey aggregates with irregular shapes sporadically cover the surfaces of mineral particles. In addition, mechanical damage could be observed from the irregular fracture surfaces at the edges of the particles. The sides of the particles presented an apparent layered stacking shape, which was considered a typical layered silicate mineral. From Figs. 13(b_1, b_2), the product roasted at 650 °C retained the layered structure, but more irregular small particles were observed on the surface. The large flakey particles in the raw ore were broken into flakes with smaller diameters. Cracks in the

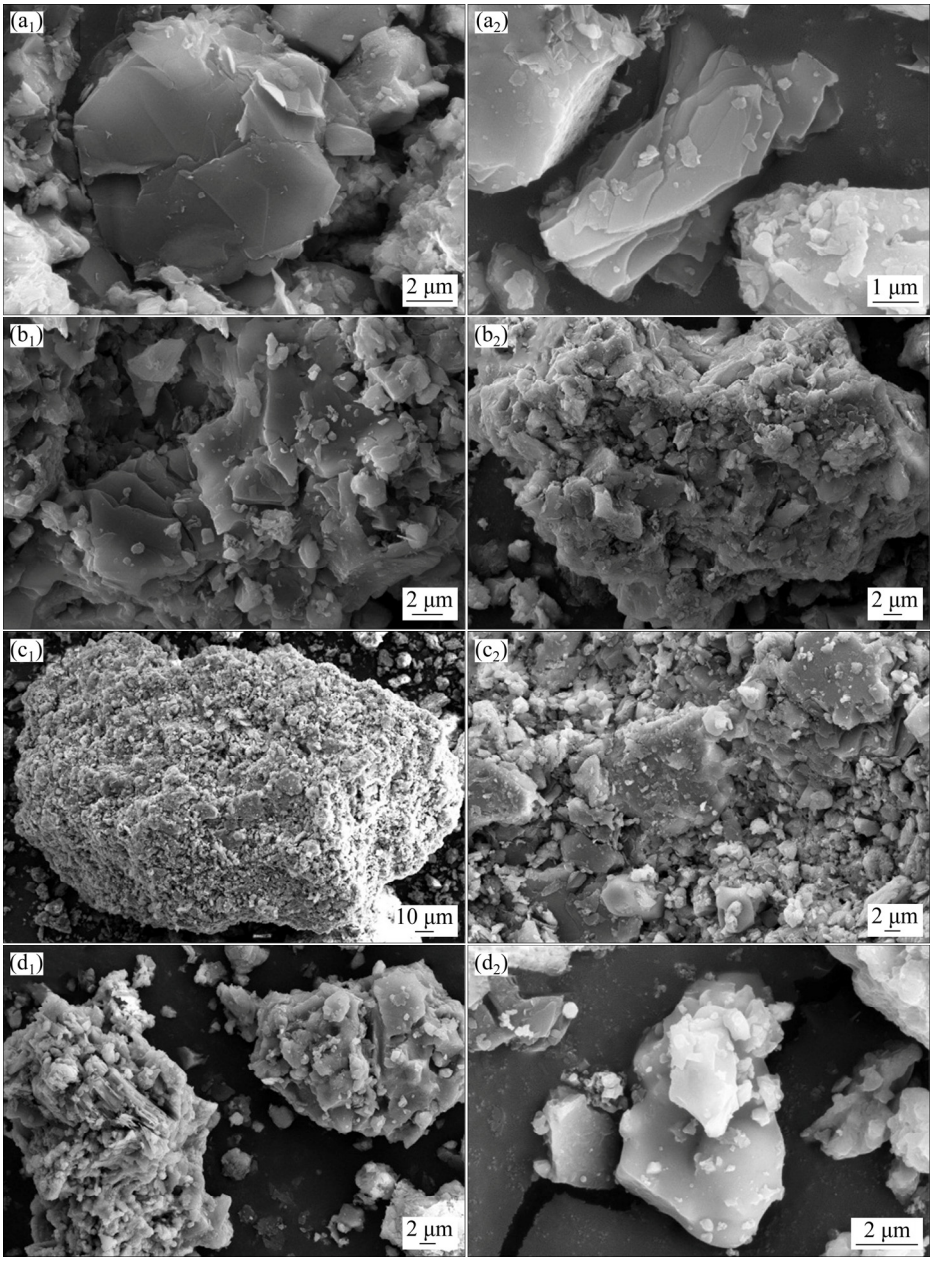

Fig. 13 Morphologies of raw ore (a_1, a_2) and roasted products of stone coal at different temperatures: (b_1, b_2) 650 °C; (c_1, c_2) 750 °C; (d_1, d_2) 850 °C

roasted flakes could be distinctly observed in the SEM images, demonstrating a slight disruption of the lamellar structure of the silicate minerals in the stone coal samples roasted at 650 °C. Figures 13(c_1, c_2) show the morphologies of the sample roasted at 750 °C. The surfaces of the particles became rougher, and numerous particles less than 1 μm appeared. The cracks extended to break the particles completely to generate an irregularly fractured surface, and the layered structure was further damaged [31,32].

Meanwhile, the roasted mineral particles became loose and porous, which was more conducive to allowing contact between the gas and solid during the roasting process and the solid–liquid reaction during subsequent leaching. The sintering phenomenon was observed in the SEM image of the stone coal product roasted at 850 °C, as shown in Figs. 13(d_1, d_2). The rough surfaces of the stone coal particles disappeared, producing a dense mass of particles bonded by the liquid phase. The surface of the sample became smooth, and the layered structure became fuzzy. The liquid phase filled many small holes to produce a structure with a large pore cavity, and the specific surface area was reduced [31,32]. This compact film not only

weakened the effect of oxidation roasting but also seriously restrained the leaching of vanadium.

4 Conclusions

(1) The carbon in the stone coal is burned, producing CO_2 in sufficient oxygen during roasting. The difficulty order of the same type of vanadate generated by different metal oxides and V_2O_5 was $Na_2O > CaO > MgO > Fe_2O_3$. The difficulty order of the different vanadates generated by metal oxides and V_2O_5 was orthovanadate > pyrovanadate > metavanadate.

(2) The mass loss occurred mainly from 600 to 840 °C during the stone coal roasting process. The conversion ratio rose rapidly. The thermal decomposition reaction rate of stone coal increased to the peak at approximately 700 °C. The peak gradually moved to the high-temperature region with increasing heating rate. According to the verification of the FWO method and KAS method, the thermal decomposition reaction of stone coal during roasting could be better described by the Ginstling−Brounshtein equation. The apparent activation energy and preexponential factors were 136.09 kJ/mol and 12.40 s^{-1}, respectively.

(3) The goethite in stone coal slowly decomposed into hematite with increasing the temperature. The ilmenite in stone coal lost hydroxyl groups and produced dehydrated illite at 650 °C. With increasing temperature, the structure of sericite began to be destroyed, and the surface of the stone coal became rough and irregular. However, when the roasting temperature exceeded 850 °C, serious sintering occurred, and the newly formed liquid phase covered the surface of the stone coal to inhibit the leaching of vanadium.

Acknowledgments

This work was supported by the Fundamental Research Funds for the Central Universities of China (No. N2101023).

References

[1] ZHANG Yi-min, BAO Shen-xu, LIU Tao, CHEN Tie-jun, HUANG Jing. The technology of extracting vanadium from stone coal in China: History, current status and future prospects [J]. Hydrometallurgy, 2011, 109(1/2): 116−124.

[2] DAI Shi-feng, ZHENG Xue, WANG Xi-bo, FINKELMAN R B, JIANG Yao-fa, REN De-yi, YAN Xiao-yun, ZHOU Yi-ping. Stone coal in China: A review [J]. International Geology Review, 2018, 60(5/6): 736−753.

[3] HE Dong-sheng. Roasting and leaching mechanism of vanadium extraction from stone coal [M]. China: Central South University Press, 2016. (in Chinese)

[4] WANG Ming-yu, XIAO Lian-sheng, LI Qing-gang, WANG Xue-wen, XIANG Xiao-yan. Leaching of vanadium from stone coal with sulfuric acid [J]. Rare Metals, 2009, 28: 1−4.

[5] JIANG Mou-feng, Study on mechanism of extracting vanadium by blank roasting and acid leaching from mica-type stone coal [D]. Wuhan: Wuhan University of Technology, 2015. (in Chinese)

[6] HU Yang-jia, ZHANG Yi-ming, BAO Shen-xu, LIU Tao. Effects of the mineral phase and valence of vanadium on vanadium extraction from stone coal [J]. International Journal of Minerals, Metallurgy, and Materials, 2012, 19(10): 893−898.

[7] LIU Xin, ZHANG Yi-min, LIU Tao, CAI Zhen-lei, SUN Kun. Pre-concentration of vanadium from stone coal by gravity using fine mineral spiral [J]. Minerals, 2016, 6(3): 82.

[8] YU Jian-wen, QIN Yong-hong, GAO Peng, HAN Yue-xin, LI Yan-jun. An innovative approach for determining the grinding media system of ball mill based on grinding kinetics and linear superposition principle [J]. Powder Technology, 2021, 378: 172−181.

[9] ZHAO Yun-liang, ZHANG Yi-min, LIU Tao, CHEN Tie−jun, BIAN Ying, BAO Shen-xu. Pre-concentration of vanadium from stone coal by gravity separation [J]. International Journal of Mineral Processing, 2013, 121: 1−5.

[10] WANG Li, SUN Wei, ZHANG Qing-peng. Recovery of vanadium and carbon from low-grade stone coal by flotation [J]. Transactions of Nonferrous Metals Society of China, 2015, 25(11): 3767−3773.

[11] WANG Li, SUN Wei, LIU Run-qing, GU Xiao-chuan. Flotation recovery of vanadium from low-grade stone coal [J]. Transactions of Nonferrous Metals Society of China, 2014, 24(4): 1145−1151.

[12] LIU Chun, ZHANG Yi-min, BAO Shen-xu. Vanadium recovery from stone coal through roasting and flotation [J]. Transactions of Nonferrous Metals Society of China, 2017, 27(1): 197−203.

[13] JIN Jian-ping, HAN Yue-xin, LI Hui, HUAI Yang-yang, PENG Yong-jun, GU Xiao-tian, YANG Wei. Mineral phase and structure changes during roasting of fine-grained carbonaceous gold ores and their effects on gold leaching efficiency [J]. Chinese Journal of Chemical Engineering, 2019, 27(5): 1184−1190.

[14] ZENG Xi, WANG Fang, ZHANG Hui-feng, CUI Li-jie, YU Jian, XU Guang-wen. Extraction of vanadium from stone coal by roasting in a fluidized bed reactor [J]. Fuel, 2015, 142: 180−188.

[15] DU Guang-chao, FAN Chuan-lin, YANG Hai-tao, ZHU Qing-shan. Selective extraction of vanadium from pre-oxidized vanadium slag by carbochlorination in fluidized bed reactor [J]. Journal of Cleaner Production, 2019, 237: 117765.

[16] TANG Zhi-dong, ZHANG Qi, SUN Yong-sheng, GAO Peng, HAN Yue-xin. Pilot-scale extraction of iron from flotation tailings via suspension magnetization roasting in a mixture of

CO and H_2 followed by magnetic separation [J]. Resources, Conservation and Recycling, 2021, 172: 105680.
[17] SUN Yong-sheng, ZHU Xin-ran, HAN Yue-xin, LI Yan-jun, GAO Peng. Iron recovery from refractory limonite ore using suspension magnetization roasting: A pilot-scale study [J]. Journal of Cleaner Production, 2020, 261: 121221.
[18] ZHANG Xiao-long, HAN Yue-xin, SUN Yong-sheng, LI Yan-jun. Innovative utilization of refractory iron ore via suspension magnetization roasting: A pilot-scale study [J]. Powder Technology, 2019, 352: 16−24.
[19] YUAN Shuai, XIAO Han-xin, YU Tian-yi, LI Yan-jun, GAO Pao. Enhanced removal of iron minerals from high-iron bauxite with advanced roasting technology for enrichment of aluminum [J]. Powder Technology, 2020, 372: 1−7.
[20] YUAN Shuai, Wang Ruo-feng, GAO Pao, HAN Yue-xin, LI Yan-jun. Suspension magnetization roasting on waste ferromanganese ore: A semi-industrial test for efficient recycling of value minerals [J]. Powder Technology, 2022, 396: 80−91.
[21] ZHU Yang-ge, ZHANG Guo-fan, FENG Qi-ming, LU Yi-ping, OU Le-ming, HUANG Si-jie. Acid leaching of vanadium from roasted residue of stone coal [J]. Transactions of Nonferrous Metals Society of China, 2010, 20(1): 107−111.
[22] LI Hong-yi, WANG Kang, HUA Wei-hao, YANG Zhao, ZHOU Wang, XIE Bing. Selective leaching of vanadium in calcification-roasted vanadium slag by ammonium carbonate [J]. Hydrometallurgy. 2016, 160: 18−25.
[23] WANG Tai-ying, XU Long-jun, LIU Chen-lun, ZHANG Zhao-di. Calcified roasting-acid leaching process of vanadium from low-grade vanadium-containing stone coal [J]. Chinese Journal of Geochemistry, 2014, 33(2): 163−167.
[24] WANG Fei, ZHANG Yi-min, LIU Tao, HUANG Jing, ZHAO Jie, ZHANG Guo-bin, LIU Juan. Comparison of direct acid leaching process and blank roasting acid leaching process in extracting vanadium from stone coal [J]. International Journal of Mineral Processing, 2014, 128: 40−47.
[25] ZHANG Cheng-qiang, SUN Chuan-yao, LI Hang, YIN Wan-zhong, ZHOU Jun-jie. Blank roasting kinetics of illite type vanadium bearing stone coal [J]. Journal of Materials Research and Technology, 2020, 9(4): 7363−7369.
[26] FENG Ya-li, CAI Zhen-lei, LI Hao-ran, DU Zhu-wei, LIU Xin-wei. Fluidized roasting reduction kinetics of low-grade pyrolusite coupling with pretreatment of stone coal [J]. International Journal of Minerals, Metallurgy, and Materials, 2013, 20(3): 221−227.
[27] HU Rong-zu, GAO Sheng-li, ZHAO Feng-qi, SHI Qi-zheng, ZHANG Tong-lai, ZHANG Jian-jun. Thermal analysis dynamics [M]. 2nd Edition. China: Science Press, 2008. (in Chinese)
[28] YUAN Shuai. Basic research on Preparation of calcined kaolin by Suspension Calcination and activation of coal gangue [D]. Shenyang: Northeastern University, 2018. (in Chinese)
[29] JI Yi-long, SHEN Shao-bo, LIU Jian-hua, XUE Yuan. Cleaner and effective process for extracting vanadium from vanadium slag by using an innovative three-phase roasting reaction [J]. Journal of Cleaner Production, 2017, 149: 1068−1078.
[30] ZHAO Yun-liang, ZHANG Yi-min, SONG Shao-xian, CHEN Tie-jun, BAO Shen-xu. Behaviors of impurity elements Ca and Fe in vanadium-bearing stone coal during roasting and its control measure [J]. International Journal of Mineral Processing, 2016, 148: 100−104.
[31] YUAN Shuai, LI Yan-jun, HAN Yue-xin, GAO Peng. Effects of carbonaceous matter additives on kinetics, phase and structure evolution of coal-series kaolin during calcination [J]. Applied Clay Science, 2018, 165: 124−134.
[32] ZHAO Yun-liang, WANG Wei, ZHANG Yi-min, SONG Shao-xian, BAO Shen-xu. In-situ investigation on mineral phase transition during roasting of vanadium-bearing stone coal [J]. Advanced Powder Technology, 2017, 28(3): 1103−1107.

含钒石煤的悬浮焙烧过程：特性表征、热力学、动力学

袁 帅[1,2]，秦永红[1,2]，金永朋[1,2]，李艳军[1,2]

1. 东北大学 资源与土木工程学院，沈阳 110819；
2. 国家地方难选铁矿资源高效开采技术联合工程研究中心，沈阳 110819

摘 要：系统地研究含钒石煤在悬浮焙烧过程中的热力学、动力学、物相转化和微观结构演变。热力学计算表明，在焙烧过程中，石煤中的碳在氧气充足的情况下燃烧并生成 CO_2，石煤的主要质量损失区间为 600～840 ℃，热分解反应速率在700 ℃左右达到峰值。通过Flynn−Wall−Ozawa(FWO)和Kissinger−Akahira−Sunose(KAS)方法验证，石煤的热分解反应由Ginstling−Brounshtein方程描述，表观活化能和指数前因子分别为136.09 kJ/mol和12.40 s^{-1}。石煤中的伊利石在650 ℃时失去羟基，产生脱水伊利石，绢云母结构被逐渐破坏。随着温度的升高，石煤表面变得粗糙且不规则，焙烧温度为850 ℃时烧结严重。

关键词：含钒石煤；热力学；热分解动力学；物相转变；微观结构演化

(Edited by Bing YANG)